Methods for Digital Restoration of Signals Degraded by a Stochastic Impulse Response

PATRICK L. COMBETTES, STUDENT MEMBER, IEEE, AND H. JOEL TRUSSELL, MEMBER, IEEE

Abstract—**In this paper, several digital restoration methods are extended to the cases in which signals have suffered stochastic blurring. Rather than being regarded in terms of averages, these degradations are treated dynamically in the derivation of restoration algorithms based on various mathematical criteria. It is shown that the integration of the additional uncertainties caused by the variations of the impulse response of the stochastic degradation can be used to obtain better estimates. These uncertainties can be included in the restoration scheme in a very flexible manner through the use of the Projection Onto Convex Sets (POCS) method. Conventional constrained methods are also addressed. The benefits of the method are illustrated through one- and two-dimensional simulations.**

I. Introduction

VERY often, signals have been recorded in the presence of one or more sources of degradation and the information they carry is not readily available to the user. It is the purpose of digital signal restoration to produce the best estimate of the original signal, according to some mathematical criterion, given the recorded data and some *a priori* knowledge.

Most restoration techniques are based on deterministic signal degradation models, i.e., models where the impulse response is represented by a mathematical function that is either completely specified *a priori* or assumed to be precisely measurable *a posteriori*. In such a framework, signals are physical quantities subjected to well-defined transformations that model their form in perfectly predictable ways. However, an actual signal, e.g., a two-dimensional image, is very often formed as a result of one or more stochastic processes and its restoration requires statistical treatment. For instance, the basic interaction of light and matter is fundamentally a statistical phenomenon which cannot be predicted in advance. Whenever an object is viewed through a medium which is not a vacuum, such as the Earth's atmosphere, random fluctuations of the index of refraction can seriously degrade the image and statistical methods are needed to quantify the degradations caused by the stochastic point spread function (psf). Another example is found in X-ray imaging, where the image formed by a phosphor screen-film system results from the stochastic amplification and the random scattering of quanta. The restoration of images degraded by deterministic linear motion blur is well understood. However, in many situations, an image can be blurred by random motions.

In the past, the restoration of stochastically blurred signals has often been approached in terms of averages without considering the variations of the impulse response. We shall show that the integration of the additional uncertainties caused by the stochastic impulse response can be used to obtain better estimates.

Manuscript received July 14, 1987; revised June 16, 1988.

The authors are with the Department of Electrical and Computer Engineering, North Carolina State University, Box 7911, Raleigh, NC 27695.

IEEE Log Number 8825655.

II. Stochastic Versus Deterministic Signal Restoration

A deterministic restoration relies on the exact knowledge of the impulse response of the degradation. Moreover, in such a framework, the only uncertainty resides in the noise, which is usually modeled in the signal formation equation by a random signal-independent additive component.

The degradations which are of interest here are stochastic in that they arise through a process which is developing in time in a manner controlled by probabilistic laws. In the restoration techniques which are developed, the knowledge about the degradation is purely statistical. For instance, the first and second moments of the psf may be available or may be determined from the data *a posteriori*. Alternatively, in a discrete environment, we may be able to describe the stochastic degradation by a collection of transition probabilities which govern the formation of the degraded signal. Stochastic analysis allows construction of models based on statistical assumptions which are inherently more flexible and general (indeed, they contain the deterministic model as a special case).

Using conventional notation, the discrete linear signal formation model can be written as

$$\boldsymbol{d} = \boldsymbol{H}\boldsymbol{a} + \boldsymbol{n} \tag{1}$$

where $\boldsymbol{d}$ is the recorded signal of length, N, $\boldsymbol{H}$ a single realization of the stochastic impulse response matrix ($N \times N$), $\boldsymbol{a}$ the original signal of length N, and $\boldsymbol{n}$ zero mean stationary signal-independent noise of length N. In this model, the stochastic impulse respone H has unknown variations about its mean $\overline{H}$

$$H = \overline{H} + \Delta H \quad \text{where} \quad \overline{H} = EH. \tag{2}$$

It is assumed that $\overline{H}$ is shift invariant. The variations, however, may represent a space-variant process. For in-

0096-3518/89/0300-0393$01.00 © 1989 IEEE

stance, the variations of the psf of a turbulent atmosphere can be considered space invariant if the observation angle is small. For large angles, the variations are space variant. Nonstationarity of the psf is also observed in the case of X-ray scatter.

III. The Set Theoretic Approach in Signal Restoration

Because the set theoretic approach is well suited for the restoration of stochastic blurs, it will be briefly reviewed. The underlying mathematical concepts regarding set properties and Hilbert spaces can be found in [3] and [8].

Set theoretic methods for signal restoration obtain a solution which is consistent with all the available information. In [12], such a solution is called a feasible solution. It is desired to use sets for defining the solution because almost all pieces of *a priori* knowledge can be modeled as a set C_i in the signal space Ω where $\boldsymbol{a}$ lies. Suppose that the *a priori* information consists of m constraints, each of which is associated with a set in Ω. A feasible solution is therefore any element in the intersection set

$$C_0 = \bigcap_{i=1}^{m} C_i. \tag{3}$$

If Ω is a metric space, the effectiveness of the restoration can be measured by the topological diameter of C_0, i.e., the supremum of the distance between any two of its elements [3]. It is noted that a feasible solution is not necessarily unique. Now suppose that the signal space Ω is a Hilbert space and that the m subsets $C_1, \cdots, C_m$ used in the description of the solution are closed and convex. Then the method of sequential projections onto (closed) convex sets (POCS) can be employed to obtain a feasible solution, i.e., an element of C_0. This method was first introduced in [2], and we now proceed to present it.

Let C be a closed and convex set in a Hilbert space $(\Omega, \|\cdot\|)$. The projection onto C of a vector z of Ω is the unique vector $\boldsymbol{x}_p$ of C which satisfies

$$\|z - \boldsymbol{x}_p\| = \inf_{x \in C} \{\|z - \boldsymbol{x}\|\}. \tag{4}$$

We shall assume that C_0 is not empty. Let P_i be the projection operator onto C_i. Consider the sequential algorithm

$$\boldsymbol{a}^{(k+1)} = P\boldsymbol{a}^{(k)} \quad \text{where} \quad P = \prod_{i=1}^{m} P_i. \tag{5}$$

Although P is not the projection operator onto C_0, it can be shown that, for any initial $\boldsymbol{a}^{(0)}$, the above iteration converges weakly to some $\hat{\boldsymbol{a}}$ in C_0; in Euclidean spaces, the convergence is strong [2]. The algorithm is stopped at the kth iteration if it yields a vector $\boldsymbol{a}^{(k)}$ in C_0. This vector is in accordance with all the available *a priori* knowledge modeled as closed convex sets, and thus it is a feasible solution.

In our application, the signal space Ω is simply the Hilbert space R^N endowed with the standard scalar product inducing the Euclidean norm $\|\cdot\|$. The POCS method was first applied to signal restoration in [9] and [14]. Examples of useful closed and convex sets are given there. In [12] it was pointed out that statistical constraints based on the residual could be used to construct sets. Indeed, if we suppose that H is known, the residual associated with (1) is defined by

$$\boldsymbol{r} = \boldsymbol{d} - H\hat{\boldsymbol{a}} \tag{6}$$

where $\hat{\boldsymbol{a}}$ represents the restored signal. From (1) and (6), it is clear that if the original signal is perfectly recovered $\boldsymbol{a} = \hat{\boldsymbol{a}}$, and therefore $\boldsymbol{r} = \boldsymbol{n}$. The noise is unknown, but in many applications its statistics are available and they should be in agreement with the sample statistics of the residual. Examples on sets based on this principle can be found in [12] and will be employed later.

IV. Processing of Stochastic Signal Degradations

The most basic approach to the problem of finding an estimate $\hat{\boldsymbol{a}}$ is to use conventional deterministic methods (minimum mean-square error (MMSE), maximum entropy (ME), constrained least-squares, etc.), where the operator H is replaced by $\overline{H}$. Such techniques, where the effects of the stochastic impulse response H are quantified in terms of its mean, will be referred to as static restoration methods. In static restoration methods, all the random variables (r.v.) involved in the description of the stochastic operator H are degenerate. On the other hand, we shall say that a restoration technique is dynamic if it takes into account the possibly nonstationary variations of the impulse response about its mean value and therefore allows a broader class of signals to be acceptable as a solution. For instance, it has been shown in [10] that the MMSE criterion could be extended to the cases in which the degradation operator is random. In the discrete frequency domain, the expression of the stochastic linear Wiener filter reads [10]

$$Q(k) = \frac{P_a(k)\, EH^*(k)}{P_a(k)\, E\left|H(k)\right|^2 + P_n(k)} \tag{7}$$

where * superscript denotes complex conjugates, P_a is the power spectrum of the original image, and P_n is that of the noise. It is noted that such a restoration filter includes the second moment of the psf. In general, a dynamic restoration scheme requires more probabilistic knowledge about the degradation operator than just its mean. Recently, the stochastic restoration problem has been approached by expressing the estimate $\hat{\boldsymbol{a}}$ of the original signal $\boldsymbol{a}$ as a weighted superposition of shifted versions of the degraded signal $\boldsymbol{d}$ [13]. The weights were then computed to optimize a cost function based on a tradeoff between resolution and noise. In this procedure, the stochastic impulse response is assumed to be uncorrelated and its mean has to be known.

In this section, the focus will be on quantifying the effects of a stochastic degradation operator. The additional

uncertainty caused by the unknown variations of H can be included in the restoration scheme in a very flexible manner through the use of iterative methods such as the POCS method. In order to take these variations into account, we shall derive an expression for the parameters which are used to define the closed convex sets associated with residual-based constraints. Then, it will be seen that any constrained restoration technique can benefit from this extension and examples will be discussed in Section IV-C. It will be assumed that the general linear model which is given by (1) holds and that, in addition, the noise is uncorrelated.

A. Sample Variance of the Residual

The requirement that the squared Euclidean norm of the residual vector $\boldsymbol{r}$ be equal to the expected value of that of the noise vector $\boldsymbol{n}$ has been used in several restoration methods. Let σ^2 be the variance of the noise. From (6), the constraint reads

$$\| \boldsymbol{d} - H\hat{\boldsymbol{a}} \|^2 = E\| \boldsymbol{n} \|^2 = N\sigma^2. \tag{8}$$

This constraint can be satisfied using the closed convex set defined by [12]

$$C_v' = \left\{ \hat{\boldsymbol{a}} \,\middle|\, \| \boldsymbol{d} - H\hat{\boldsymbol{a}} \|^2 \le \delta_v \right\} \quad \text{where} \quad \delta_v = N\sigma^2. \tag{9}$$

The projection of a vector not in the set belongs to its boundary and therefore produces a residual which satisfies the equality constraint (8). It is noted that since in our case only $\overline{H}$ is known, the residual which is available is

$$\boldsymbol{r} = \boldsymbol{d} - \overline{H}\hat{\boldsymbol{a}}. \tag{10}$$

By inspecting (1) and (2), it is seen that if $\hat{\boldsymbol{a}}$ were exactly $\boldsymbol{a}$, we would get

$$\boldsymbol{r} = \boldsymbol{n} + \Delta H\boldsymbol{a} = \boldsymbol{n}' \tag{11}$$

where $\boldsymbol{n}'$ can be regarded as the new noise vector consisting of the original noise plus a term which accounts for the unknown variations of the stochastic impulse response about its mean. Therefore, the constraint is written as

$$\| \boldsymbol{r} \|^2 = E\| \boldsymbol{n}' \|^2 = E(\boldsymbol{n} + \Delta H\boldsymbol{a})^T(\boldsymbol{n} + \Delta H\boldsymbol{a}). \tag{12}$$

Since the processes $\boldsymbol{n}$ and $\Delta H\boldsymbol{a}$ are uncorrelated and zero mean, the expansion yields

$$\| \boldsymbol{r} \|^2 = \delta_v + E\| \Delta H\boldsymbol{a} \|^2 = \delta_v'. \tag{13}$$

Clearly, the bound has increased over its value in the deterministic case δ_v by a factor which is the contribution of the stochastic blur. Generally speaking, a stochastic degradation operator introduces more uncertainty in the system, and this uncertainty propagates through the derivations of an estimate $\hat{\boldsymbol{a}}$, and will eventually increase the diameter of the set of feasible solutions. In practice, the theoretical factor δ_v' in (13) is not tractable because probabilistic information about $\Delta H\boldsymbol{a}$ is not available and we have to deal with the norms of ΔH and $\hat{\boldsymbol{a}}$ individually. We have

$$E\| \Delta H\boldsymbol{a} \|^2 \le \| \boldsymbol{a} \|^2 E\| \Delta H \|^2. \tag{14}$$

The evaluation of $E\| \Delta H \|^2$ requires some discussion. Let $\beta = E\| \Delta H \|^2$ and

$$\Delta H = [\Delta h_{kn}]_{N\times N}. \tag{15}$$

Since $\| \cdot \|$ represents the Euclidean norm for vectors, the associated matrix norm is the spectral norm whose square is given by

$$\| \Delta H \|^2 = \max_k \{ \lambda_k \} \tag{16}$$

where λ_k is the kth eigenvalue of $\Delta H^T \Delta H$. If we assume that the variations of the impulse response are shift invariant, then ΔH can be approximated by a circulant matrix [1], and it is therefore diagonalized by the Discrete Fourier Transform (DFT) operator W where

$$W = \left[\exp\left(-j\frac{2\pi}{N} kn \right) \right]_{N\times N}. \tag{17}$$

Thus, we obtain the following diagonal matrix:

$$\Lambda_{\Delta H^T \Delta H} = W[\Delta H^T]\, W^{-1} W[\Delta H] W^{-1}. \tag{18}$$

Its kth element is simply $\lambda_k = |\, \Delta H(k) \,|^2$, where $\Delta H(k)$ is the kth component of the DFT of the sequence $\{ \Delta h(n), 0 \le n \le N-1 \}$. By construction, the r.v.'s $\Delta h(n)$ have mean zero and, if we further assume that they are uncorrelated, they are orthogonal. It follows at once that for each k in $\{0, 1, \cdots, N-1\}$, the r.v.'s $\{ X_n = \Delta h(n) \exp[-j(2\pi/N)kn], 0 \le n \le N-1 \}$ are also orthogonal and therefore,

$$E\left| \sum_{n=0}^{N-1} X_n \right|^2 = \sum_{n=0}^{N-1} E|X_n|^2 \tag{19}$$

which entails

$$(\forall k \in \{0, 1, \cdots, N-1\}) E\lambda_k = E|\Delta H(k)|^2 = \sum_{n=0}^{N-1} E|\Delta h(n)|^2. \tag{20}$$

Thus, we get

$$\beta = E\| \Delta H \|^2 = \sum_{n=0}^{N-1} E|\Delta h(n)|^2. \tag{21}$$

Furthermore, the authors have found empirically that in cases when the variations of the impulse response are shift variant, the above expression could be modified to

$$\beta = \max_k \left\{ \sum_{n=0}^{N-1} E|\Delta h_{kn}|^2 \right\} \tag{22}$$

and produce a useful bound. Hence, the parameter computed in actuality for C_v is

$$\zeta_v = \delta_v + \beta\| \boldsymbol{a} \|^2. \tag{23}$$

The values of $\delta_{r'}'$ and $\zeta_{r'}$ will be computed for a practical example in Section V. Thus, the set associated with the noise variance constraint reads

$$C_{r'} = \left\{ \hat{\boldsymbol{a}} \,\middle|\, \| \boldsymbol{d} - \overline{H}\hat{\boldsymbol{a}} \|^2 \leq \zeta_{r'} \right\}. \tag{24}$$

B. Power Spectral Bounds

It is desired to constrain the power spectrum of the residual to match that of the noise process $\boldsymbol{n}'$ of (11), which we denote by $P_{n'}$. In practice, the periodogram of the residual will be used as an estimator of its power spectrum. It is observed that the periodogram is an inconsistent estimator but it is easily computed and modified. In [12], the set for the deterministic case was constructed by assuming that the noise component in (1) is white and Gaussian. Consequently, the residual should enjoy the same property and its periodogram will therefore have a chi-square distribution with two degrees of freedom for discrete frequencies strictly between 0 and $N/2$ [7]. Thus, given a confidence interval, a confidence factor α can be derived for the normalized r.v. defined as [7]

$$p(k) = \frac{2\left| R(k) \right|^2}{N\sigma^2} \quad \text{for} \quad 0 < k < \frac{N}{2}. \tag{25}$$

Let δ_p be defined as

$$\delta_p = \frac{\alpha N}{2}\sigma^2. \tag{26}$$

The closed convex set associated with the constraint is given by [12]

$$C_p = \left\{ \hat{\boldsymbol{a}} \,\middle|\, \left| D(k) - H(k)\,\hat{A}(k) \right|^2 \leq \delta_p, \quad \text{for} \quad 0 < k < \frac{N}{2} \right\}. \tag{27}$$

We need to see how the set is modified in the stochastic case. To this end, consider the variations of the stochastic impulse response H in the frequency domain

$$H(k) = \overline{H}(k) + \Delta H(k). \tag{28}$$

In cases where H is stationary, (1) yields a set of decoupled equations in the frequency domain. Clearly, if the stochastic impulse response is shift variant, the matrix relation in (1) no longer represents convolution. In such instances, a frequency domain representation is not appropriate. From (10), the DFT samples of the residual based on the mean impulse response read

$$R(k) = D(k) - \overline{H}(k)\,\hat{A}(k). \tag{29}$$

And, from (11), if $\boldsymbol{a}$ were perfectly recovered we would get

$$R(k) = N(k) + \Delta H(k)\,A(k) = N'(k). \tag{30}$$

Since the processes $\boldsymbol{n}$ and $\Delta H\boldsymbol{a}$ are uncorrelated and zero mean,

$$P_{n'}(k) = P_n(k) + P_{\Delta Ha}(k) = \sigma^2 + P_a(k)\,E\left| \Delta H(k) \right|^2. \tag{31}$$

Given a confidence limit, the confidence factor α can be computed by regarding the noise process of (11) as white and Gaussian. In general, this assumption is inexact but it permits us to establish a bound on $|R(k)|^2$ which has proven acceptable in practice

$$\delta_p'(k) = \delta_p + \frac{\alpha N}{2} P_a(k)\,E\left| \Delta H(k) \right|^2. \tag{32}$$

Therefore, a collection of sets is created as follows:

$$C_p^{(k)} = \left\{ \hat{\boldsymbol{a}} \,\middle|\, \left| D(k) - \overline{H}(k)\,\hat{A}(k) \right|^2 \leq \delta_p'(k) \right\} \quad \text{for} \quad 0 < k < \frac{N}{2}. \tag{33}$$

It is noted that, as opposed to the static bound δ_p, the bound $\delta_p'(k)$ is frequency dependent. Under the assumption that the $\Delta h(n)$'s are uncorrelated, the value of $E|\Delta H(k)|^2$ can be obtained by using (20). If it is known that they are not, then additional context-dependent information can be used to determine the spectral behavior of the degradation operator. For instance, in the case of turbulence-degraded images, it is well known [4] that in the near field all the blur arises from statistically describable phase perturbations. A general account of the statistical properties of the optical transfer function of a random propagation medium is given in [6].

Let us also note that because the noise sequence defined in (11) is signal dependent, so are the parameters which define the sets in (24) and (33), and therefore these sets do not have a fixed boundary. Because the POCS algorithm of (5) operates on fixed sets, it is necessary to render $\zeta_{r'}$ and the $\delta_p'(k)$'s independent from $\boldsymbol{a}$ by assigning constant values to $\| \boldsymbol{a} \|$ and the $P_a(k)$'s (the value of $\| \boldsymbol{a} \|$ represents no more information than is in its power spectrum P_a, which is required for MMSE restoration and can be estimated by similar methods when it is not already available from a prototype signal or other *a priori* knowledge). Convergence to a realistic solution is thereby guaranteed.

Other sets based on the statistics of the residual, such as those given in [12], can be derived in a like manner; for example, mean of the residual, outliers of the residual.

C. General Constrained Methods

As was mentioned previously, constrained restoration techniques can be reformulated to include the variations of the impulse response. In this respect, let us consider the constrained ME and least-squares problems. In both cases, the constraint is [1]

$$\| \boldsymbol{d} - H\hat{\boldsymbol{a}} \|^2 = \delta_{r'}. \tag{34}$$

As was done before, since only $\overline{H}$ is known, by considering the new noise process $\boldsymbol{n}'$, the constraint becomes that of (13). Again, in practice, the bound $\zeta_{r'}$ will be used in lieu of the exact (but mathematically untractable) value $\delta_{r'}'$, and it will admittedly lead to a more conservative filter. Nonetheless, $\zeta_{r'}$ will produce a more realistic estimate

than the smaller value δ_v which would lead to an inverse filtering operation, as will be seen in Section IV-D. From (23), the dynamic constraint reads

$$\| \boldsymbol{d} - \overline{H}\hat{\boldsymbol{a}} \|^2 = \zeta_v = \delta_v + \beta \| \hat{\boldsymbol{a}} \|^2. \tag{35}$$

Consequently, the conventional constrained ME problem [1] is modified to

$$\underset{\text{over } \hat{\boldsymbol{a}}}{\text{minimize}} \left\{ \hat{\boldsymbol{a}}^T \ln \{\hat{\boldsymbol{a}}\} \right\} \quad \text{subject to}$$
$$\| \boldsymbol{d} - \overline{H}\hat{\boldsymbol{a}} \|^2 = \delta_v + \beta \| \hat{\boldsymbol{a}} \|^2. \tag{36}$$

A straightforward Lagrangian minimization yields

$$\ln \{\hat{\boldsymbol{a}}\} = \mu(\overline{H}^T\boldsymbol{d} + [\beta I - \overline{H}^T\overline{H}]\hat{\boldsymbol{a}}) - \mathbf{1} \tag{37}$$

where the Lagrange multiplier μ is adjusted so that the equality constraint of (35) is satisfied. It is noted that the ME formulation of (36) makes the incorporation of the variations of H easy. The definition of the ME problem given in [5] does not lend itself to such a modification.

The dynamization procedure for the constrained least-squares problem is similar to that followed above. Thus, the conventional formulation of the constrained least-squares problem [1] is modified to

$$\underset{\text{over } \hat{\boldsymbol{a}}}{\text{minimize}} \left\{ \| C\hat{\boldsymbol{a}} \| \right\} \quad \text{subject to}$$
$$\| \boldsymbol{d} - \overline{H}\hat{\boldsymbol{a}} \|^2 = \delta_v + \beta \| \hat{\boldsymbol{a}} \|^2. \tag{38}$$

Using the method of Lagrange multipliers and the appropriate circularity assumptions, the estimate in the discrete frequency domain will be given by

$$\hat{A}(k) = \frac{D(k)\, EH^*(k)}{\left| EH(k) \right|^2 + \gamma \left| C(k) \right|^2 - \beta} \tag{39}$$

where γ is the reciprocal of the Lagrange multiplier associated with (35). It is worth noting that the static counterpart of these dynamic algorithms is obtained as a particular case for $\beta = 0$.

D. The Benefits of a Dynamic Procedure

We have seen that the dynamic parameters of the sets associated with the constraints on the sample variance of the residual and on the spectral bounds of its power spectrum were, respectively, defined in the dynamic case by

$$\begin{cases} \delta_v' = \delta_v + E \| \Delta H \hat{\boldsymbol{a}} \|^2 \\ \delta_p'(k) = \delta_p + \dfrac{\alpha N}{2} P_a(k)\, E \left| \Delta H(k) \right|^2. \end{cases} \tag{40}$$

The difference from the static case lies in the addition of a term depending on the variations of the stochastic degradation operator H, be it in the signal domain for C_v or in the frequency domain for $C_p^{(k)}$. This inclusion of the variations of H increases the diameter of the convex sets and, as a result, that of the set of feasible solutions. In that respect, the following point should be strongly emphasized: when a static procedure is followed, the set of feasible solutions is smaller than that obtained through dynamic processing, and it may seem that the problem is better defined in the former case. However, the set of solutions yielded by a dynamic procedure will contain the true solution, which may not be the case when a static method is employed. In other words, the dynamic solution set has been enlarged in order to contain all the original signals that may have produced the observed data. This point can be illustrated by considering the static constraint

$$\| \boldsymbol{d} - \overline{H}\hat{\boldsymbol{a}} \|^2 = \delta_v. \tag{41}$$

If we assume that the variance of the noise is very small, the estimate is the pseudoinverse solution which is a very poor estimate because $\overline{H}$ is the average operator and is certainly not equal to the operator H which generated the data $\boldsymbol{d}$. On the other hand, if the dynamic equality constraint associated with (13) is used, a realistic solution will be obtained. Finally, it should be noted that if the signal has been formed in a very noisy environment, and if the variance of the impulse response is small, the terms δ_v and δ_p will be dominant in (40) and the dynamic parameters will be almost equal to their static counterpart so that no improvement over a static restoration should be expected.

Other sets can be used as an efficient means to incorporate additional information to the algorithm: set of nonnegative signals, band-limited signals set, along with other sets mentioned in [14]. In addition, it has appeared to the authors that a minimum entropy constraint also yields a closed and convex set which could be of great use.

V. Experimental Results

In this section, we shall present examples of restoration of signals degraded by a random impulse response and noise. Both 1-D and 2-D signals will be considered. The stochastic Wiener filter of (7) along with the static and the dynamic POCS methods will be applied to these signals. The projection operators onto C_v and the $C_p^{(k)}$'s will be obtained from (4). They will be similar to that derived in [12] and need not be reproduced here.

A. One-Dimensional Simulations

The original signal $\boldsymbol{a}$ is $N = 256$ points in length and is shown in Fig. 1. A single realization stochastic impulse response $h(n)$ is created as follows: M points are generated at random locations, between -128 and 127. The location of a point is a zero mean Gaussian-distributed r.v. with a standard deviation of 8. The nth value of the stochastic impulse response, i.e., $h(n)$, is obtained by counting the number of points which fall in the interval $[n - 0.5,\ n + 0.5]$. Therefore, the probability that a point falls at the location of the nth point is

$$p_n \approx \frac{1}{8\sqrt{2\pi}} \exp\left(-\frac{n^2}{128}\right) \tag{42}$$

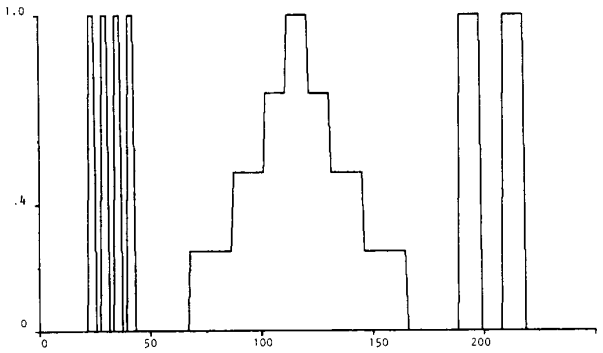


Fig. 1. The original signal.

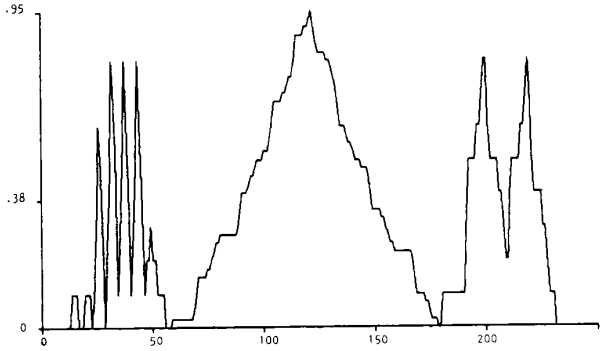


Fig. 2. Blurred signal—$M = 10$.

and

$$\sum_{n=-N/2}^{N/2-1} p_n \approx 1. \tag{43}$$

The probability density function of $h(n)$ is simply a binomial distribution

$$P\{h(n) = m\} = \binom{M}{m} p_n^m (1 - p_n)^{M-m}. \tag{44}$$

The impulse response is then normalized in order to model a lossless linear system, i.e., $\Sigma_n h(n) = 1$. Therefore, $Eh(n) = p_n$, and Var $h(n) = p_n(1 - p_n)/M$. As the total number of points M increases, the impulse response $h(n)$ approaches the average Gaussian impulse response $Eh(n)$.

Circular convolution is implemented in the frequency domain to blur the original signal $\boldsymbol{a}$, and therefore H is circulant. Figs. 2–4 show the blurred signals for various values of the parameter M. The signal convolved with the average impulse response $Eh(n)$ appears in Fig. 5. The degraded signals are created by adding zero mean, stationary, white Gaussian noise to the blurred signals. For the simulations we present here, the variance of the noise σ^2 was chosen to obtain a signal-to-noise ratio of 30 dB. The midrange value $M = 100$ is chosen to demonstrate the effects of a stochastic impulse response. The signal degraded by this impulse response and the noise is displayed in Fig. 6. The static parameter δ_v was computed to be equal to 0.06326.

The value of ζ_v needed to define C_v can be determined from (23) by noting that

$$E\left|\Delta h(n)\right|^2 = \text{Var } h(n) = \frac{p_n(1 - p_n)}{M}. \tag{45}$$

Since ΔH is circulant, (21) yields

$$\beta = \frac{1}{M}\left(1 - \sum_{n=-N/2}^{N/2-1} p_n^2\right). \tag{46}$$

Table I gives the exact value of δ_v', as computed directly from $\boldsymbol{a}$, $\bar{H}$, and a particular realization of the stochastic process H for various values of M, along with the corre-

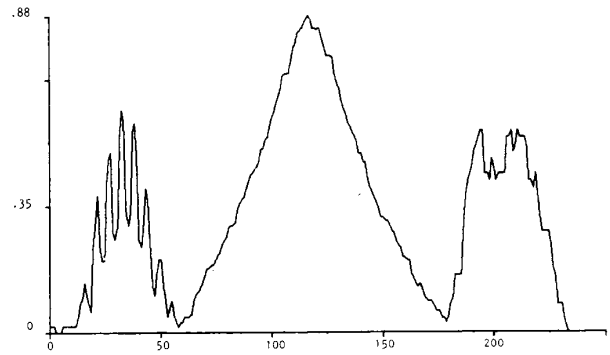


Fig. 3. Blurred signal—$M = 50$.

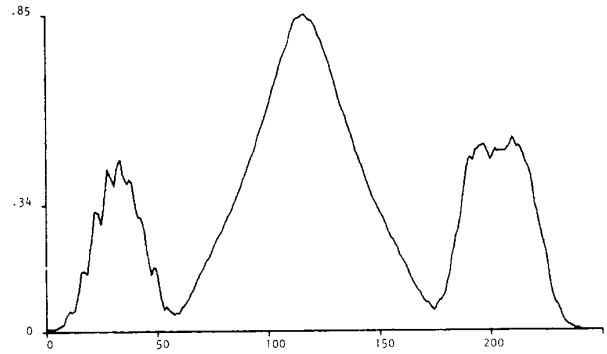


Fig. 4. Blurred signal—$M = 500$.

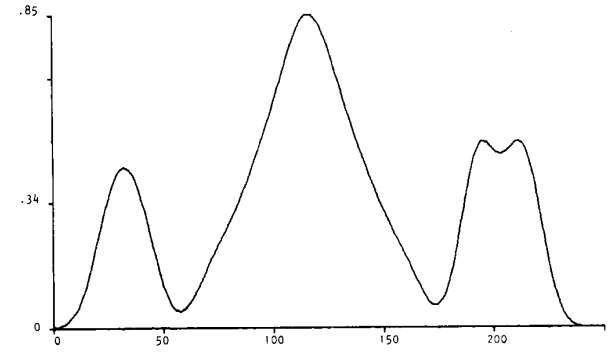


Fig. 5. Signal blurred with the average impulse response.

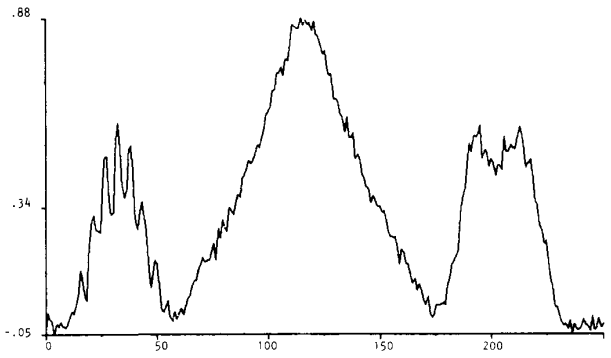


Fig. 6. Degraded signal.

TABLE I
δ_v' AND ζ_v AS A FUNCTION OF M

M	δ_v'	ζ_v
10	.84854	6.1972
30	.50134	2.1080
100	.34039	.67666
300	.15697	.26773
1000	.07277	.12460
3000	.06845	.08371
10000	.06515	.06939
30000	.06441	.06530

sponding value of ζ_v. It is noticed that δ_v' and ζ_v decrease as M increases since the instantaneous impulse response approaches its average. Moreover, by looking at the value of the static parameter δ_v, which appears in (9) and which depends only upon the noise, it is clear that for small values of M, the variations of the impulse are overwhelming.

To project onto C_p, we first need to determine the static value of δ_p. The confidence limit on $|R(k)|^2$ was set to 99 percent, which led to $\delta_p = 0.2913$. The value of $E|H(k)|^2$ needed to compute $\delta_p'(k)$ in (32) can be determined as follows:

$$E\left|H(k)\right|^2 = E\left|\Delta H(k)\right|^2 + \left|EH(k)\right|^2 = \beta + \left|P(k)\right|^2 \quad (47)$$

where β is as in (46) and where $P(k)$ represents the kth component of the DFT of the sequence $\{p_n, -N/2 \leq n < N/2\}$ defined in (42). Fig. 7 shows the frequency dependence of $\delta_p'(k)$ as computed exactly from $\boldsymbol{a}$, $\overline{H}$, and a particular realization of H for two values of M.

The stochastic Wiener filter was used to produce the estimate seen in Fig. 8. The term $EH^*(k)$ in (7) is simply $P^*(k)$ and $E|H(k)|^2$ is given in (47). Then the conventional static POCS filter was used and the restored signal is displayed in Fig. 9. The estimate was obtained by projecting sequentially onto the sets C_v and C_p, where static parameters were used, and C_n, the closed convex set of nonnegative signals. The static POCS technique fails to converge because the diameters of C_v and C_p are both too small and C_0 is empty.

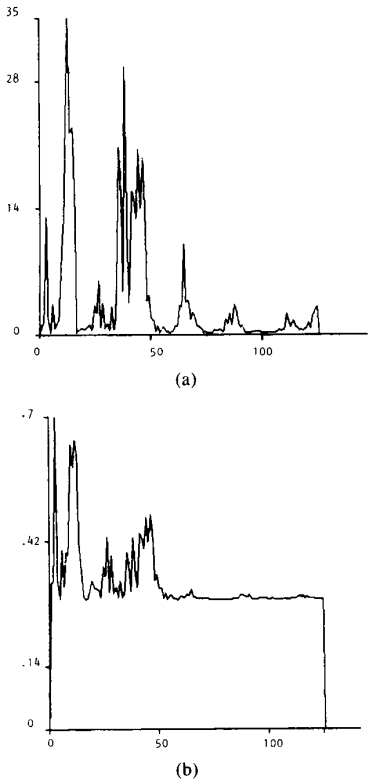


Fig. 7. $\delta_p'(k)$ as a function of the frequency. (a) $M = 10$; (b) $M = 2000$.

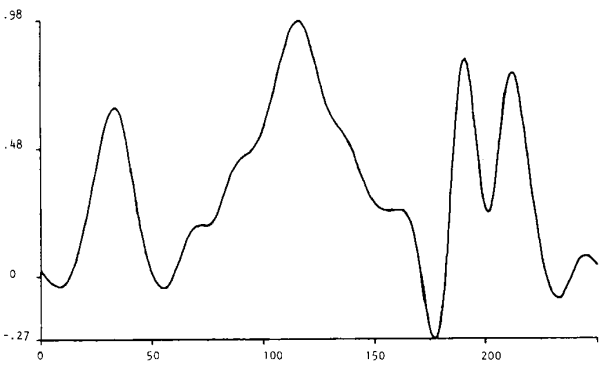


Fig. 8. Restored with the stochastic Wiener filter.

The dynamic POCS method was employed: sequential projections were performed onto the dynamic convex sets: C_v, $C_p^{(k)}$, and C_n. A confidence interval of 99 percent was used to project onto $C_p^{(k)}$. The restored signal was obtained in 9 iterations and is seen in Fig. 10. For both POCS methods, the degraded signal was used as an initial estimate. The POCS resolved the rightmost peaks better than the stochastic Wiener. Finally, let us note that if the number of points M is small, the terms involving ΔH are very large and, therefore, the diameter of the intersection of the sets will be large. As a result, the algorithm will not modify the initial estimate a great deal, and not much improvement should be expected. On the other hand, if

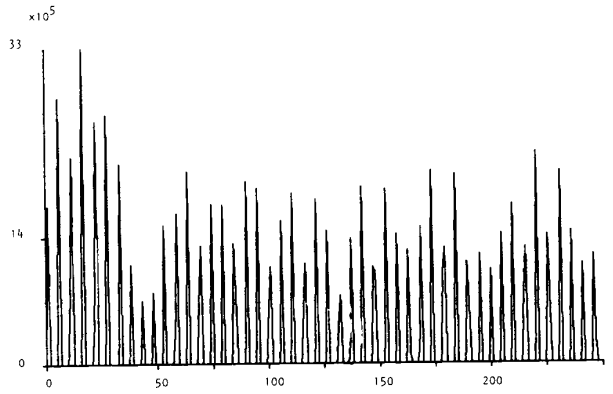


Fig. 9. Restored with the static POCS filter.

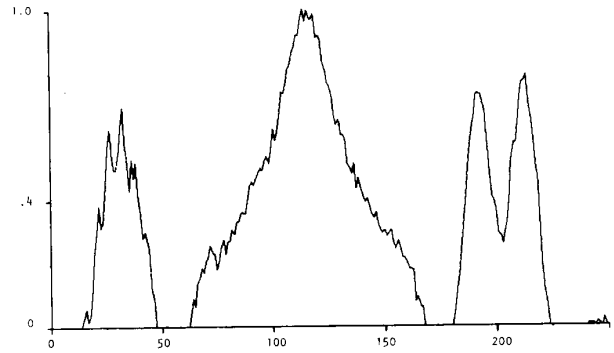


Fig. 10. Restored with the dynamic POCS filter.

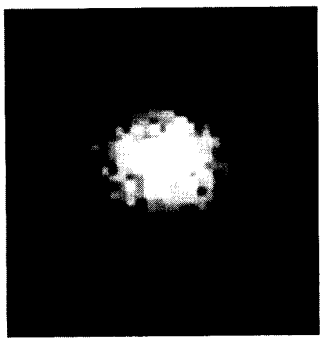


Fig. 11. Stochastic PSF, $M = 3000$.

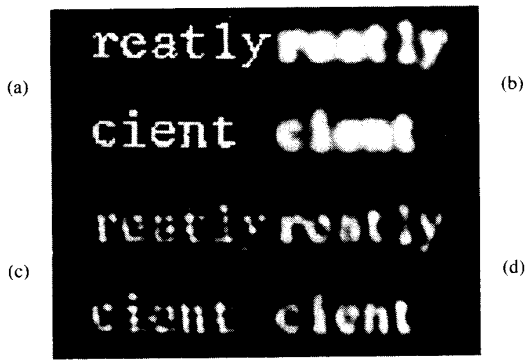


Fig. 12. Restoration, $M = 1000$. Upper left (a) original; upper right (b) degraded; lower left (c) stochastic Wiener; lower right (d) dynamic POCS.

M is large, one might as well perform average processing since the variations of the impulse response H about its mean are minimal.

B. Two-Dimensional Simulations

The stochastic point spread function $h(m, n)$ was obtained as a 2-D extension of the impulse response $h(n)$: the value of $h(m, n)$ is equal to the number of points falling in the area $[m - 0.5, m + 0.5] \times [n - 0.5, n + 0.5]$. The images used in these simulations are 128×128. Since the Gaussian r.v.'s m and n are statistically independent and identically distributed, they can be generated separately. We present results for which a standard deviation of 4 pixels was chosen. The average psf $Eh(m, n)$ is therefore the zero-mean circularly symmetric 2-D Gaussian distribution, with a variance of 16. An example of stochastic psf is given in Fig. 11, where 3000 points were generated (for better observation, the psf has been magnified three times). This psf resembles examples of short-exposure atmospheric psf given in [6]. It could also be regarded as the pattern obtained by scattering a single point with a photon count of 3000 in an X-ray image.

The original image of Fig. 12(a) was blurred by implementing circular convolution, and therefore the degradation which is simulated here is assumed to be spatially invariant. A stationary, zero-mean, Gaussian white noise with variance corresponding to a signal-to-noise ratio of 30 dB was added to the image blurred with the stochastic psf generated with $M = 1000$ points. This degraded image is seen in Fig. 12(b). The value of the static factor δ_p was computed as earlier, with a confidence limit of 99 percent. The static POCS filter diverged, as it did in the 1-D case. The image restored by the stochastic Wiener filter is shown in Fig. 12(c). The negative lobes have been removed from the image for display (part of the *a priori* knowledge about the original image is that all the pixel values are nonnegative). This solution displays several regions where an undue amount of energy has accumulated. Sequential projections were performed onto the dynamic convex sets: C_v, $C_p^{(k,l)}$, where k and l represent the spatial DFT frequencies, and C_n to produce the restoration seen in Fig. 12(d), and for which the degraded image was used as an initial estimate. The POCS iterations converged in 10 iterations. The distribution of the energy for this solution, as opposed to that of the Wiener solution, is more faithful to the original. Compared to Fig. 12(c), the estimate of Fig. 12(d) is smoother and visually more pleasing.

At this point, it was noted that, because of the particular distribution of the energy in the original image, a maximum power constraint could prove very useful in order to improve the resolution of the restored image. In addition, introducing a maximum power constraint is a good opportunity to demonstrate the flexibility of the

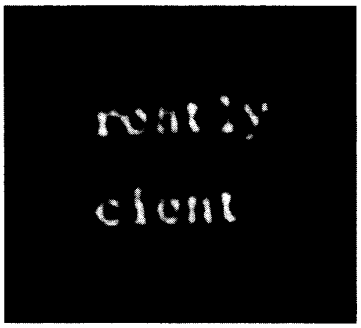


Fig. 13. Restored image, $M = 1000$. Dynamic POCS with maximum power constraint.

POCS method with regard to the incorporation of additional *a priori* knowledge. The maximum power constraint was included to the dynamic POCS algorithm by increasing the power after each projection by 10 percent until the total was 80 percent of the original image, according to the procedure discussed in [11]. The result of this process is shown in Fig. 13 and was obtained in 8 iterations. A significant improvement in sharpness is noticed: the thickness of the letters is quite comparable to that of the original.

VI. Conclusions

The general linear stochastic blur problem has been treated. Several restoration algorithms have been discussed and compared to techniques using only static or average impulse responses. It was seen that in order to achieve satisfactory results, the variations of the stochastic degradation operator must be incorporated to the algorithm as part of the *a priori* knowledge. We have shown how this could be done for the POCS method as well as for conventional constrained restoration techniques (e.g., maximum entropy, constrained least-squares).

Both 1-D and 2-D restorations have been carried out based on the modified POCS method, where the dynamics of the degradation operator H is considered. By incorporating these variations rather than by performing average processing, the diameter of the sets used to define the solution increases to a point where we are virtually certain that their intersection contains a true solution. The set theoretic stochastic restoration methods could be further improved by the inclusion of additional *a priori* information about the solution in specific applications.

References

[1] H. C. Andrews and B. R. Hunt, *Digital Image Restoration*. Englewood Cliffs, NJ: Prentice-Hall, 1977.

[2] L. M. Brègman, "The method of successive projection for finding a common point of convex sets," *Doklady Akademiia Nauk SSSR*, vol. 162, pp. 487-490, 1965. (English translation in *Soviet Mathematics—Doklady*, vol. 6, no. 3, pp. 688-692, May 1965.)

[3] Jean Dieudonné, *Foundations of Modern Analysis*, 2nd ed. New York: Academic, 1969.

[4] D. L. Fried, "Optical resolution through a randomly inhomogeneous medium for very long and very short exposures," *J. Opt. Soc. Amer.*, vol. 56, no. 10, pp. 1372-1379, Oct. 1966.

[5] B. R. Frieden, "Restoring with maximum likelihood and maximum entropy," *J. Opt. Soc. Amer.*, vol. 62, no. 4, pp. 511-518, Apr. 1972.

[6] J. W. Goodman, *Statistical Optics*. New York: Wiley Interscience, 1985.

[7] G. M. Jenkins and D. G. Watts, *Spectral Analysis and Its Applications*. Oakland, CA: Holden Day, 1968.

[8] D. G. Luenberger, *Optimization by Vector Space Methods*. New York: Wiley, 1969.

[9] M. I. Sezan and H. Stark, "Image restoration by the method of convex projections: Part 2—Applications and numerical results," *IEEE Trans. Med. Imaging*, vol. MI-1, pp. 95-101, Oct. 1982.

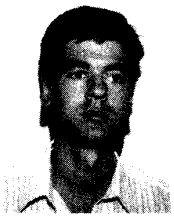
[10] D. Slepian, "Linear least-squares filtering of distorted images," *J. Opt. Soc. Amer.*, vol. 57, no. 7, pp. 918-922, July 1967.

[11] H. J. Trussell, "Maximum power signal restoration," *IEEE Trans. Acoust., Speech, Signal Processing*, vol. ASSP-29, pp. 1059-1061, Oct. 1981.

[12] H. J. Trussell and M. R. Civanlar, "The feasible solution in signal restoration," *IEEE Trans. Acoust., Speech, Signal Processing*, vol. ASSP-32, pp. 201-212, Apr. 1984.

[13] R. K. Ward and B. E. A. Saleh, "Deblurring random blur," *IEEE Trans. Acoust., Speech, Signal Processing*, vol. ASSP-35, pp. 1494-1498, Oct. 1987.

[14] D. C. Youla and H. Webb, "Image restoration by the method of convex projections: Part 1—Theory," *IEEE Trans. Med. Imaging*, vol. MI-1, pp. 81-94, Oct. 1982.



Patrick L. Combettes (S'84) was born in Salon de Provence, France, on May 24, 1962. He received the Diplôme d'Ingénieur from l'Institut National des Sciences Appliquées de Lyon, France, in June 1985 and the M.S. degree from North Carolina State University in January 1987, both in electrical engineering.

He is conducting his Ph.D. studies in the Department of Electrical and Computer Engineering at North Carolina State University, where he is a Research Assistant. His primary interests include digital signal processing, probability theory, and aerobics.

Mr. Combettes is a member of Phi Kappa Phi, the IEEE Acoustics, Speech, and Signal Processing Society, and the American Mathematical Society.



H. Joel Trussell (S'74-M'76) was born in Atlanta, GA, on February 3, 1945. He received the B.S. degree from Georgia Tech in 1967, the M.S. degree from Florida State in 1968, and the Ph.D. degree from the University of New Mexico in 1976.

He joined the Los Alamos Scientific Laboratory, Los Alamos, NM, in 1969 where he began working on image and signal processing in 1971. During 1978-1979, he was a Visiting Professor at Heriot-Watt University, Edinburgh, Scotland. In 1980 he joined the Electrical and Computer Engineering Department at North Carolina State University, Raleigh. His current interests include signal restoration/reconstruction and mathematical methods.

Dr. Trussell has won the IEEE-ASSP Society Senior Paper Award (with M. R. Civanlar). He is currently an Associate Editor for the IEEE Transactions on Acoustics, Speech, and Signal Processing, and a member of the Multidimensional Digital Signal Processing Committee of that Society. He is a member of Sigma Xi, Tau Beta Pi, Phi Kappa Phi, and the Signal Processing Society.

A Scanning and Sampling Scheme for Computationally Efficient Algorithms of Computer Tomography

KEVIN D. DONOHUE, MEMBER, IEEE, AND JAFAR SANIIE, MEMBER, IEEE

Abstract—**This paper presents a scanning and sampling scheme for computerized tomography that reduces the number of required interpolations in the reconstruction algorithm. Hence, the computational load associated with interpolation is also reduced. For the case where no restrictions are placed on the sampling rates of the scanner, a set of projection angles along with their corresponding sampling rates are derived such that no interpolation is required to calculate the final image points for the display grid. From this result a reduced interpolation scheme is developed for the case when upper and lower bounds exist on the sampling rates. A discussion is presented on the choice of an optimal set of projection angles that will maintain an image quality comparable to a sampling scheme of regular measurement geometry, while minimizing the computational load. The Cartesian-grid scanning and sampling (CGSS) scheme developed here is compared to a sampling scheme of regular measurement geometry through a computer simulation. The results demonstrate that for higher sampling rates and images of limited pixel dimension, the CGSS scheme can reduce the computational load of the reconstruction process and maintain comparable image quality.**

I. INTRODUCTION

THE field of computerized tomography (CT) has generated much interest in reconstructing two-dimensional images from their sampled projections. This imaging process can be thought of in three stages. First is the data acquisition stage, which determines how the object will be scanned and exactly what samples will be taken. The second stage is the reconstruction algorithm that processes these samples to obtain image points. Finally, the reconstructed image must be displayed. This is usually done on a Cartesian grid. For data acquisition, the two basic projections are the parallel beam and the fan beam [1]. For either type of projection, the actual position of the detectors will determine the arrangement of samples in the Fourier domain. The reconstruction algorithm must be adapted to accept the particular set of samples determined by the scanning and sampling geometry [2]–[6]. In the last stage, the algorithm must take the processed samples and perform interpolation to estimate the value of the discrete points on the Cartesian grid.

Given the general configuration for parallel- or fan-beam projections, different sampling schemes can be created by variations of the projection angles and sampling rates on each projection. In a typical parallel-beam scanner, an array of evenly spaced detectors positioned along a straight line (projection axis) measures the attenuation of a beam perpendicular to the detector array, which has traversed through the object (Fig. 1). This is done for every evenly spaced position along the projection axis. Then the whole axis is rotated about the center of the object by a fixed angular increment and the measurements are repeated. This type of geometry is referred to as a polar raster because the Fourier space in this case is sampled in an arrangement of concentric circles. A variation on this geometry was developed in previous work [7] to find a set of sampling rates that yields concentric squares in the sampled Fourier space (thus referred to as a concentric squares raster). This simplified the interpolation in the frequency domain to prepare the samples for a direct Fourier inversion. The technique not only reduced calculations, but also improved the image quality over that of the polar raster. Another scan and sample geometry was proposed for backprojection algorithms, which uses variable scanning steps coupled with a sampling rate that varies from scan to scan to eliminate interpolation from the reconstruction algorithm. This technique resulted in a reduction in the computational load for image reconstruction [8].

This paper presents a derivation of the set of special projection angles with corresponding sampling rates for parallel-beam projections that causes the reconstruction algorithm to calculate points that directly contribute to the image. The sampling scheme is derived from the geometry of the Cartesian grid so that the samples fed into the algorithm contain more information about the points of interest than the samples that must be interpolated for the display. The application of this scan and sample geometry to the filtered-backprojection algorithm is presented in the next section. A complete set of projection angles along with their corresponding sampling rates, which yield interpolation-free results, is derived for this algorithm. In

Manuscript received August 1, 1986; revised June 16, 1988. The work of the first author was supported by a fellowship from the American Electronics Association, while the author was in the Department of Electrical and Computer Engineering at the Illinois Institute of Technology.

K. D. Donohue was with the Department of Electrical and Computer Engineering, Illinois Institute of Technology, Chicago, IL. He is now with the Department of Electrical and Computer Engineering, Drexel University, Philadelphia, PA 19104.

J. Saniie is with the Department of Electrical and Computer Engineering, Illinois Institute of Technology, Chicago, IL 60616.

IEEE Log Number 8825664.

0096-3518/89/0300-0402$01.00 © 1989 IEEE

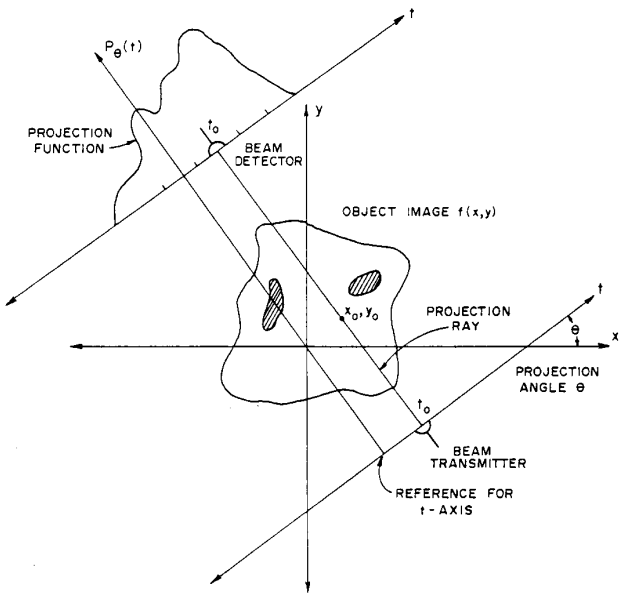


Fig. 1. Typical arrangement for a parallel-beam projection measurement. The function $P_\theta(t)$ represents the measurement of attenuation for each projection ray emitted from the projection axis at position t.

Section III, the choice of an optimal set of angles, which minimize computational effort while maintaining comparable image quality, is discussed. Since some of the required sampling rates for a given projection may be very high, a procedure is developed to find the best set under the constraint of upper and lower bounds for the sampling rates. In these cases a limited amount of interpolation is required. Finally, the results of a computer simulation compare the Cartesian-grid scanning and sampling (CGSS) scheme to the polar raster of regular measurement geometry and conclusions are drawn.

II. Development of an Interpolation-Free Projection Set

The filtered-backprojection algorithm reconstructs a cross-sectional image of an object from its backprojection data. The cross-sectional image of an object can be reconstructed from its projections [1] by

$$f(x, y) = \int_0^{\pi} \int_{-\infty}^{+\infty} S_\theta(\nu) |\nu| e^{j2\pi\nu t} \, d\nu \, d\theta \qquad (1)$$

where $f(x, y)$ is the reconstructed image in the x-y plane, and $S_\theta(\nu)$ is the Fourier transform of the projection, $P_\theta(t)$, taken at angle θ

$$S_\theta(\nu) = \int_{-\infty}^{+\infty} P_\theta(t) e^{-j2\pi\nu t} \, dt \qquad (2)$$

where t represents the position along the projection axis corresponding to image points that intersect the path of the projection ray in the x-y plane (see Fig 1). For a given projection angle, θ, the image points are related to the position t along the projection axis by

$$t = x \cos\theta + y \sin\theta. \qquad (3)$$

Now let

$$Q_\theta(t) = \int_{-\infty}^{+\infty} S_\theta(\nu) |\nu| e^{j2\pi\nu t} \, d\nu \qquad (4)$$

where $Q_\theta(t)$ is referred to as the filtered-backprojection. The substitution of (3) and (4) into (1) results in

$$f(x, y) = \int_0^{\pi} Q_\theta(x \cos\theta + y \sin\theta) \, d\theta. \qquad (5)$$

Since there are a finite number of samples available, (5) must be expressed in discrete form. If the projections of the object are considered approximately band-limited to some frequency less than B, and N samples span each projection, then (2) is approximated by

$$S_\theta(\nu) \approx \frac{1}{2B} \sum_{k=-N/2}^{+N/2} P_\theta\left(\frac{k}{2B}\right) e^{-j2\pi\nu k/2B} \qquad (6)$$

and an approximation for (4) can be written as

$$Q_\theta\left(\frac{k}{2B}\right) \approx \frac{2B}{N} \sum_{m=-N/2}^{N/2} S_\theta\left(m \frac{2B}{N}\right) \left| m \frac{2B}{N} \right| e^{j2\pi mk/N}. \qquad (7)$$

Error is introduced in the samples of $Q_\theta(t)$ due to the band-limited approximation. Since the image is spatially finite, the spectral information in the frequency components that exceed twice the sampling frequency result in aliasing error. This error is distributed throughout the spectral domain. To reduce this error, the image can be sampled at a higher rate, which decreases the amount of spectral energy contributing to this error.

Since only a finite number of projections is processed, the integral of (5) can be approximated (rectangular formula) by

$$f(x, y) \approx \frac{\pi}{I_p} \sum_{i=1}^{I_p} Q_{\theta_i}(x \cos\theta_i + y \sin\theta_i) \qquad (8)$$

where Q_{θ_i} is the filtered-backprojection at angle θ_i and I_p is the total number of projections. The error associated with the approximation of (8) is discussed in the next section and in Appendix A.

Now if the reconstructed image is to be displayed on a Cartesian grid, then only a finite number of points are of interest. For every reconstructed point (x_0, y_0), a corresponding value of $Q_{\theta_i}(t_{0,i})$ must be found for all θ_i, where $t_{0,i}$ is related to x_0, y_0, and θ_i by (3). In (7), if $k/2B \neq t_{0,i}$ for some integer k and projection angle θ_i, then interpolation is required to obtain that value of $Q_{\theta_i}(t_{0,i})$. With some forethought, projection angles and sampling rates can be chosen such that

$$t_{k,i} = k\tau_i = x_l \cos\theta_i + y_m \sin\theta_i \qquad \text{for all integers } k \qquad (9)$$